Supplemental Document

A Third Angular Momentum of Photons

Pathik Sahoo[1,2], Pushpendra Singh[1,2], Jhimli Manna[2], Ravindra P. Singh[3], Jonathan P. Hill[1], Tomonobu Nakayama[1], Subrata Ghosh[4,5] and Anirban Bandyopadhyay[1*,]

[1]*International Center for Materials Nanoarchitectronics (MANA), NIMS, 1-2-1 Sengen, Tsukuba, Ibaraki-3050047, Japan.*
[2]*Research Center for Advanced Measurement and Characterization (RCAMC), NIMS, 1-2-1 Sengen, Tsukuba, Ibaraki-3050047, Japan.*
[3]*Quantum Science & Technology Laboratory, Physical Research Laboratory, Navrangpura, Ahmedabad, Gujarat 380009, India.*
[4]*Chemical Science and Technology Division, CSIR-North East Institute of Science and Technology, NEIST, Jorhat, Assam, 785006, India.*
[5]*Academy of Scientific and Innovative Research (AcSIR), Ghaziabad-201002, UP, India.*
 *anirban.bandyo@gmail.com

S1. Materials and Methods

A. Preparation of gelators

(S)-(+)Phenylglycine methyl ester hydrochloride (6.1 mM,1.23 g) was treated with an aqueous K_2CO_3 solution (2 M, 2 mL), and the free ester was then extracted using diethyl ether. The diethyl ether solution was placed in a two-neck 100 mL round-bottomed flask. Ether was removed under reduced pressure yielding pure (S)-(+)-phenylglycine methyl ester. At room temperature, dry THF (30 mL) and then dry palmitoyl chloride (1.5 mL) were added sequentially under continuous stirring. The reaction mixture was raised to 60 °C then dry triethylamine (1.5 mL) was added to the reaction mixture. The reaction mixture formed a gelatinous mass. The solution was then heated at reflux for 2 h. and the reaction mixture was allowed to cool to room temperature and THF was removed under reduced pressure. The resulting white solid was filtered, washed with aqueous 1N HCl, aqueous 1N NaOH, and deionized water and dried under reduced pressure at 55 °C.

B. Birefringence and optical vortex study

Following the preparation of 1 wt% hexane-based gel using the established cooling procedure, a small amount of gel was carefully taken using a spatula and spread on a transparent quartz slide to test the formation of a polarization-entangled photon pair. Red laser light (@633 nm) was passed through the sample, and the slide was slowly tilted to observe angle-dependent birefringence.

As synthesis progresses, live transmission spectra map a gradual formation and population of the three resonance frequencies (Figure 2C). Furthermore, the ratios of experimental and theoretically measured frequencies are similar. The helical nanowire pitch is 1/3 of the incident photon wavelength (He-Ne laser 633 nm), as seen statistically in the thin film of nanowires on a Cu grid. The pitch-diameter ratio of nanowires maps an additional twist ω of a spiral path that imparts a third orthogonal momentum to the incident photons.

S2. Supplementary Texts

2.1 Hamiltonian of the helical nanowire assembly

To build a photon with three angular momenta, the ideal path of incident photons should have three orthogonal distributions of electron density states so that they simultaneously experience three orthogonal modulations. We use a helix as a

primary template, as shown in Figure 1B (below) to create photons having two angular momenta θ, φ. A higher order of twisting can be applied to the helix similarly to that known for DNA helices or microtubules, Figure 1C (below, twisted spiral). Consequently, we have added a third angular momentum ω by devising a method involving three orthogonal distributions of the electron density of states.

The pitch of a helical nanowire creates a periodic gap in the electron density distribution, which adds one angular momentum θ to the incident linear photon. After light-matter interaction, photons are reflected in a spiral path. However, helices possess both linear and spiral paths. A spiral motion carries two distinct continuous distributions of electron density states along the horizontal and transverse axes. The difference between the optical axis and longitudinal transmission axis causes incident photons to split into two coherent sources. Helical nanowires used here exhibit such birefringence, as do microtubules and DNA. The two resulting photons travel on distinct paths within the nanowire and have a phase gap. They interfere, and due to periodic gaps between destructive interference points, an alternate p number of bright and dark spots along the perimeter of a light ring can be observed. The resulting ring of light or vortex is called a vector vortex beam, ϕ, whose momentum is $p\hbar$. Suppose there is an additional helical twist ω in the nanowires as they self-assemble further, as shown in Figure 1B. Then, the corresponding electron density path is perpendicular to the vector beam, thus adding another spiral phase ω to the incident photon. This vector vortex beam rotates, creating a sphere, ω. Nye discussed a photon structure with a helix of a helix of a helix form; here, to derive that photonic structure, we have created a structurally similar material. Adding three momenta θ, ϕ, ω to one photon opens the door to the creation of virtual molecules composed of three geometric phases arising from representative hardware, i.e., vibrating fibers. For its spiral motion, the azimuthal index ℓ, represents the number of cycles of 2π phase developed around the circumference to deliver an orbital angular momentum of $\ell\hbar$ per photon. Azimuthal angular momentum is a scalar entity $\Psi(\theta) = Cos\theta + iSin\theta$. The larger the light ring (or vortex), the greater is the momentum. Two orthogonal rotations require a vector element $\Psi(\theta, \phi) = Cos\theta + e^{i\phi}Sin\theta$ where the greater the number of dark spots, the larger is the momentum.

The Hamiltonian that defines the energy of twisted helical nanowire and its corresponding photon condensate has four parts **H = H1 + H2 + H3 + H4** If a pair of crossing paths have n_i number of clocking waves $\vec{\psi}_{osci}$, each wave with an energy E_i, then, the total energy, filtered of noise is **H1** $= \sum_i E_i n_i^2$. The zigzag path filters noise in a strictly quantized manner. The separated energy of the clocking wave is $\Delta\varepsilon_\pm = \frac{\hbar k_F^2}{2m^*} = \pm\sqrt{2(1 - Cosk)}$, which is part of the total energy held by a pair of zigzag paths $K1$ and $K2$, is second part of **H1** $= \sum_i \frac{E_{K1-K2}}{2}((Cos\frac{\varphi}{\varphi_0})^2 + d_i^2(Sin\frac{\varphi}{\varphi_0})^2)^{1/2}$. Here, φ is the exchanged quantized flux between the paths (flux degeneracy) with respect to a flux minimum φ_0 and d_i separates the two parallel paths, k is the wave vector. The charge asymmetry between the paths holds energy **H2** $= \frac{1}{2}m^*\omega_L^2((1 + \chi)x^2) +$

$(1 - \sigma)y^2 - \frac{\omega_{02}^2}{\omega_L^2}z^2)$, where χ is anisotropy factor, here conductivity σ distinguishes the diffracted waves ω_{02}, ω_L from different paths & layers, respectively. Refracted and transmitted monochromatic light interferes; the geometric parameters; length, L; pitch P, diameter D, and lattice area ab (product of two sides of the 2D unit cell) regulate the strength of magnetic flux and geometry of magnetic vortices. It is $\mathbf{H3} = \frac{\Omega^3}{4\pi^2}(\frac{2m^*}{\hbar^2})^{\frac{3}{2}}[3\sum_i cos\theta_i + 4\prod_i cos\theta_i]$. If we twist the coil, we get a screw ($\delta = 0$; $\delta = \pi$; left handed and right handed respectively) & edge ($\delta = \pi/2$) dislocations of zigzag paths on the coil surface, the energy of the dark lines (E=0) is given by $\mathbf{H4} = \frac{k^2}{2m^*}[(ax + kx^2 sin\delta) + i(ycos\delta + zsin\delta)]$. The part $(ax + kx^2 sin\delta) + i(ycos\delta + zsin\delta)$ is solved by simplifying the defect on the coil surface, considering that a dark line is $\psi = k(ax + iy')e^{i(kz-\omega t)}$.

Including all factors here, we find the Hamiltonian $\mathbf{H}$ of the device

$\mathbf{H} = \mathbf{H1}\{\sum_i E_i n_i^2 + \frac{1}{2}m^*\omega_L^2(\{(1+\varepsilon)x^2) + (1-\mu)y^2 - \frac{\omega_{0i}^2}{\omega_{Li}^2}(z - cos\phi)^2\}$)}

$+\mathbf{H2}\sum_i \frac{E_{K1-K2}}{2}\{((Cos\frac{\varphi}{\varphi_0})^2 + d_i^2(Sin\frac{\varphi}{\varphi_0})^2)^{\frac{1}{2}}(\alpha(x_1 x_2 + x_3 x_4) + \beta(x_1 x_3 + x_2 x_4) +$

$\gamma(x_1 x_4 + x_3 x_2))\} + \mathbf{H3}\frac{\Omega^3}{4\pi^2}(\frac{2m^*}{\hbar^2})^{\frac{3}{2}}[3\sum_i cos\theta_i + 4\prod_i cos\theta_i]$ $+\mathbf{H4}\frac{K^2}{2m^*}[(ax + kx^2 sin\delta) + i(ycos\delta + zsin\delta)\dots\dots(2)$

Rotating the optical vortex or light ring about its vertical axis delivers centrifugal momentum. The light field is periodically compressed to a point with this momentum and then expands to its starting shape (Figure 1B). As p + 1, dark spots on the 2D light ring covert into dark regions on the hollow sphere $\Psi(\theta, \phi, \omega)$; we construct a function $\Gamma_i(r, t)$ that links the material and the singularity regions. Since we use a triply hierarchical supramolecular assembly of helical nanowires to modulate the diameter of the cylindrical beam (o) of spirally rotating light, three orthogonal waves interfere at each level, which leads to triplets for the sum of phases $3\sum_i cos\theta_i$. Pitch and diameter contribute to the grids on which surface charge density waves are superposed. Two variables deliver a quartet $4\prod_i cos\theta_i$, the simplest tensor that estimates the overlap. Combining these expressions gives $\Gamma_i(r, t) = 3\sum_i cosx_i + 4\prod_i cosx_i$, which represents the phase structure. The 3D plot of $\Gamma_i(r, t)$ within a boundary $(-\pi, +\pi)$ is a sphere with 12 dark regions at its surface (Figure S1b). For six of the gels studied, the areas and multiplicities of the dark regions are well defined. The corresponding tensor map of the surface profile represents the third angular momentum (Table S1). For θ, a photon's azimuthal angular momentum is $l\hbar$, for ϕ, it's radial angular momentum is $p\hbar$, for ω, centrifugal angular momentum is $o\hbar$, here (l, p, o) are topological charges. Since all twelve values on a sphere follow $-\pi \leq \Gamma_i(r, t) \leq +\pi$, the third angular momentum of the largest dark region is ~0.2$\pi\hbar$ kg m²/sec. Unlike for $\Psi(\theta)$ and $\Psi(\theta, \phi)$, for $\Psi(\theta, \phi, \omega)$ distinct symmetries with dark regions can be reshaped maintaining geometric invariance. Thus, $\Gamma_i(r, t)$ represents a new light-matter interaction.

2.2. *Optical interaction with the helical nanowire*

Controlling the adiabatic geometric phase has been achieved in optics [1]. The geometric phase is widely used to guide light [2]. Our helical nanowire shows optically induced electric and magnetic Mie resonances in dielectric nanoparticles with a high refractive index [3]. Magnetic resonance amplifies the optical signal falling on the nanosystem. The simultaneous operation of multiple grids could enable quantum superposition by squeezing the density of states, entanglement exchange, and protecting superpositions by forming artificial cavities composed of resonant modes.

Linearly propagating photons can be observed as a point of light. Spiral propagation produces a one-dimensional phase singularity, a line of undefined phase along the optical path; it yields a visible light ring (θ). An orthogonal rotation of the frontal wavelet of a spirally propagating photon creates a spiral of undefined phase; we observe alternate dark and bright spots on the projected ring of light (θ, ϕ). With one angular momentum, a line of light becomes a cylinder; with two angular momenta, the cylindrical surface acquires parallel lines of dark and bright light. Adding a third angular momentum converts the cylinder to a linear chain of hollow spheres with dark spots on its surface (θ, ϕ, ω). Spiral shaped phase singularity (θ, ϕ) now becomes discrete areas with undefined phases (θ, ϕ, ω). By manipulating θ, ϕ, ω, the geometry of dark regions could be modulated wirelessly. Each light ring or vortex making a boundary of the dark region represents a Bloch sphere or qubit and would enable physicists to synthesize optical superstructures as quantum circuits. Moreover, the capability to couple dark regions or Bloch spheres as 2D rings on the spherical surface would help resolve the topological qubit crisis and allow replication of the magnon condensate. It could also revive historical discussions regarding Maxwell's laws for magnetic monopoles.

Overlapping the dark domains of these optical 3D structures maps geometric relations between Bloch spheres. On the virtual sphere, there exist either polygons, whose vertices are composed of a framework of light columns, or circular dark regions whose perimeters are composed of light rings. For this reason, we were concerned about whether or not the optical sphere represents a classical mixture of rings or geometric shapes of light composing an illusory single structure. The derivation of a 2D light ring (θ, ϕ) from the 3D light sphere (θ, ϕ, ω) suggests that $\Psi(\theta, \phi, \omega)$ is a singular photon structure, which is further supported by its wave-like interference. The remarkable theoretical prediction of a triplet band and experimental verification should enable the generic synthesis of an optical particle that possesses volume. Birefringence generates entangled photons in helical nanowires composing an organic gel, and hydrogen-bonded nanowires within the organic gel act as single molecule-like structures. Hence geometric shapes made of coupled quantum states are editable in a particle-like photonic structure, opening up uncharted opportunities for cavity-free photonic condensates.

2.3. Measuring third angular momentum for seventeen gels

We have varied the angle of interference in H to obtain criticality where a ring-shaped field is generated. The nanowire acts as an optical polarizer twisting bundles of photons about the optical axis, creating a 'donut-like hole' at the center of the vortex. Since the length of the helical nanowire modulates the additional angular twists in the ring, seen as dark spots on the perimeters of the vortex rings in we observe vector vortex beams. The modulation of dual orbital angular momentum in an optical vortex beam can be exploited in optical communications technologies [4,5], microscopy [6,7], and quantum information processing [8,9].

Low molecular weight gelators (LMWGs) self-assemble in an appropriate solvent during cooling from a heated isotropic sol state, resulting in one dimensional (1D), two dimensional (2-D), or three dimensional (3D) network states based on weak intermolecular interactions including hydrogen bonding, halogen bonding, coordination bonding, π-π stacking, etc. Thus, during the self-assembly process, these 1D networks cross-link, yielding "junction zones"[10], and form 3D cages where solvent molecules are trapped, ending at a gel state. Simple heating of the gel erases structural information imprinted in the gel state, which can be rewritten an indefinite number of times without degradation by reforming the gel.

S3. Supplementary Figures

Figure S1
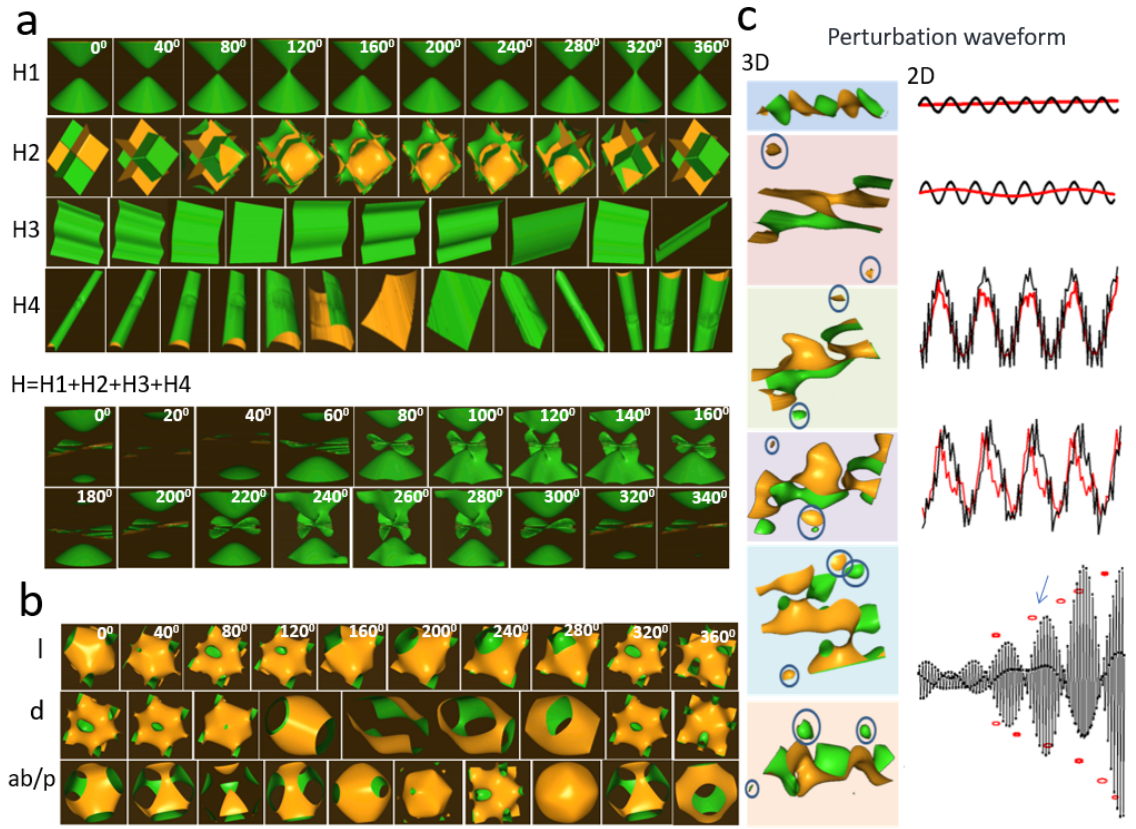
Figure S1. **Hamiltonian for gel's light-matter interaction**: The four Hamiltonian parts of the generic Hamiltonian that represent the H device are shown, and the value of the Hamiltonian is plotted against the variables concerned in those typical Hamiltonians. The 0-360 phase change for the periodically oscillating parameter shows distinct features (top). The combined Hamiltonian shows a unique behavior very different from the individual ones. (b) H3 shows a brilliant function $3\sum_i cos\theta_i + 4\prod_i cos\theta_i$ which is fundamental to the H device, the sum of cosines and product of cosines. By changing length l, diameter d, and the ratio of lattice area ab and pitch p, periodically, the number of singularities in the phase space is tuned, shown in a series of plots as a function of phase. (c) The effective dark line formed by the interaction of multi-layered helical cylinder-generated dark knots are shown where polarization and the average amplitude of perturbation signals are changed.

Figure S2
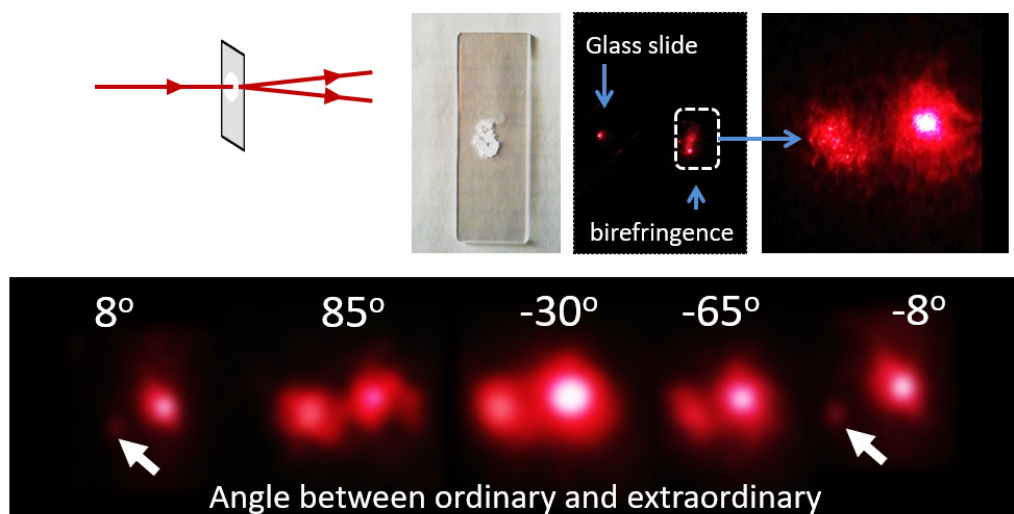
Figure S2. Angular control of birefringence: Polarized light incident on the film is split to two components only when incident at a particular angle. We either observe light that is deflected towards the optical axis or the incident light by rotating the glass slide.

Table S1. Nested Bloch spheres or Hilbert spaces for six organic gel precursors.

Each distinct gel geometry has its peculiar geometric arrangement of dark regions on the sphere. We have mapped the 3D assembly of Block spheres; each sphere represents a sub-set of the third angular momentum tensor. For each material, photon condensate does not have one but multiple values. Organogelators were synthesized according to the literature procedures: 1[11], 2[11], 3[12], 4[11,13], 5[14], 6[15], 7[16]. here the numbers depict the molecular structure in the table, in parenthesis, there are reference numbers of associated literatures.
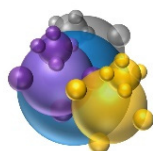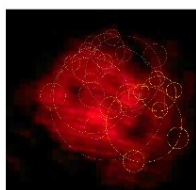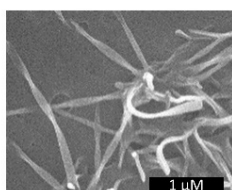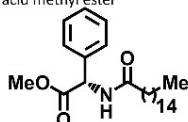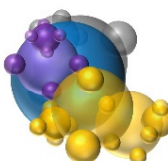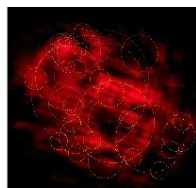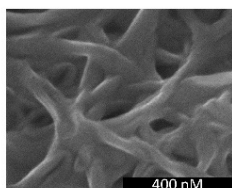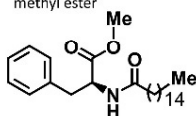
1 (S)-Phenyl-tetradecanoylamino-acetic acid methyl ester

2 µM
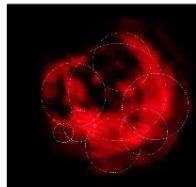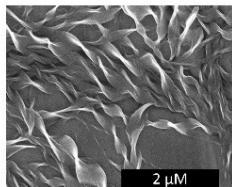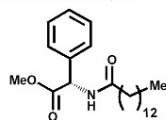
2 (R)-Phenyl-tetradecanoylamino-acetic acid methyl ester

1 µM
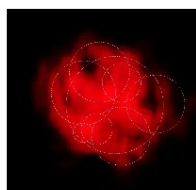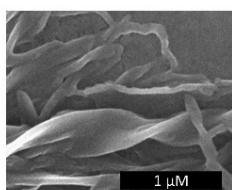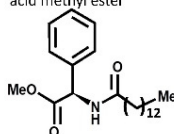
3 (S)-Phenyl-hexadecanoylamino-acetic acid methyl ester

1 µM

4 (S) 2-Hexadecanoylamino-3-phenyl-propionic acid methyl ester

400 nM

5 (S)-3-Methyl-2-hehadecanoylamino-butyric acid methyl ester

1 µM

6 {13-[(Methoxycarbonyl-phenyl-methyl)-carbamoyl]-tridecanoylamino}-phenyl-acetic acid methyl ester

1 µM

7 (S)-3-Phenyl-2-(3-p-tolyl-acryloylamino)-propionic acid methyl ester

1 µM

S4. Four Visualization descriptions

Visualization 1. Basic concept of 3rd angular momentum. Instead of a 2D template, we have used a 3D spring or helical nanowire to add first, second, and third angular momentum to a photon.

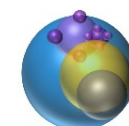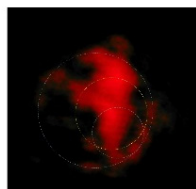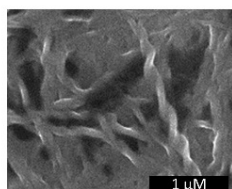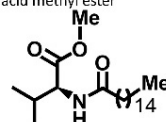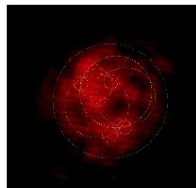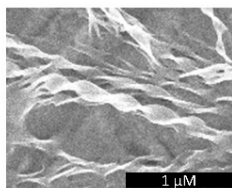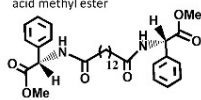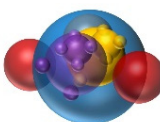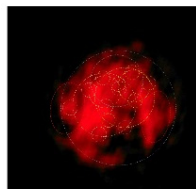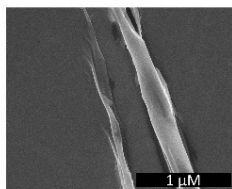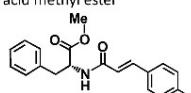*Visualization 2. Molecular dynamics of gel precursors.* The molecular precursor used is (S)-phenyl-hexadecanoylamino-acetic acid methyl ester. For gel synthesis, the precursor solution is heated and cooled. During the cooling process, the precursor molecules self-assemble to the gel state. Therefore, heat consumption is an integral part of the synthesis of the helical nanowire and self-assembled superstructure of helical nanowires. The molecular mechanics and semi-empirical calculations simultaneously yield two parameters: the molecular resonance frequencies and energy consumption while oscillating at a particular frequency. Three molecular dynamics simulation videos are provided. The first video involves a single molecule, the second video two molecules, and the third video involves three molecules.

Xenoview molecular dynamics simulation was carried out using constant volume and shape ensemble with Berendsen thermostat maintained at 298° C. Forced oscillations were induced (Forced oscillations with frequency $10/2\pi$ THz) to map resonance frequencies under available thermal energy. Natural resonance frequencies as transmission coefficients were measured to calculate eigenvectors during energy minimization. Tolerance for diagonalization is 1e-8; diffusion coefficients were calculated using random walk generating strain on the atoms. The density of states or DOS has 100 bins in the histogram.

Visualization 3: Four phase transitions for vortex condensate. This video demonstrates four phase transitions during a twisted helical nanowire synthesis. The two adjacent panels depict zoomed reaction centers spontaneously produced in the transparent solution and its corresponding contour plot. Below the two panels, we demonstrate the most likely SEM structures responsible for the three condensates. SEM structures were identified from the Histogram of nanowire clusters, where three distinct sizes of concentrates are explicit. Apart from the Histogram, we simultaneously monitored the reflected and transmitted light passing through the reaction centers and projected that on a screen. There is a one-to-one correspondence between the formation of the optical vortex with one angular momentum, two angular momenta, and three angular momenta observed in the projection camera and the reaction vessel camera. Repeated experiments were performed by melting the gel using a heat gun. The reaction vessel camera consistently shows a stable structure during three repetitions and the entire cooling process. Only for those durations did the projection camera show specific light rings. The projection camera did not show any stable structure at other times.

A high-resolution camera (1000X, 3MB, USB digital microscope, Bysameyee), kept 10 cm distant from the reaction vessel, was focused on the nucleation centers (1 cm × 1

cm cuvette) in the area (1 mm × 1 mm, light cross-section) where the light was passing through the reaction solution. Note that the reaction vessel camera focuses on the continuously growing reaction centers, capturing diffuse light emitted by the particles.

The He-Ne (633 nm, red) laser source light cross-section is 1 mm^2. In the current configuration, at ×1000 times magnification, the microscope observes a 1 μm^2 area. For reference, sunlight diffracted by dust particles amplifies luminance by 1000 times. Therefore, in principle, diffraction could make particles of 2 – 5 nm diameters visible (1 μm^2 /1000 ~ 1 nm^2) with laser diffraction. Thus, it is widely used to measure particle size [17]. Even 5 nm-sized nanoparticles have been visualized using laser light [18]. Metal nanoparticles of 4 nm – 12 nm diameters might be projected as a light sphere of 20 mm diameter (See Figure 4b and Figure 7 in the ref [19]).

We used a He-Ne laser (633 nm, 10mW) to observe the nucleation centers in the reaction vessel. Note two adjacent synchronous video screens. At the bottom, we have placed five SEM images, representing the dimensions of the structures. We have zoomed 1 mm × 1 mm, and the smallest light spot that moves on the screen is 20 – 30 μm (0.05 m, 5 s). Since the particles appear nearly 1000 times larger than their actual dimensions (Ref. [17-19], dust particles are visible in sunlight because amplification of the diffracted light is more due to coherent light). Based on calculations made elsewhere [17-19], conservative estimates suggest that the actual size of the light spot we observe might be around 20 – 30 nm. Since each molecule is around ~5 nm, we are likely observing the response due to a cluster of molecules, starting birefringences, or the generation of two coherent beams at the start of the videos.

When monitoring the diffracted light, we observe two kinds of light emerging from the reaction vessel. When nanowires diffract, emerging light has a solid light center, while if nanowires interact generating light, the emerging light spot has no light at its center, being observed as a homogeneously distributed circuit area [17-19]. The two distinct light spots visible at 0.05 min coincide, forming a combined ellipsoid of diffuse light at 0.19 min, followed by a flash of light at 0.22 min. The disappearance of light originating from diffract by individual structures and the concurrent appearance of interaction-based light output is the first sign of the large energy emission from interactions between two distinct structural elements. Furthermore, two light spots interact at 0.38 - 0.44 min, which is observed as the exchange of light spots between the two static light sources. First, we see a large flash of an emerging light spot, which disappears, generating another light spot. Subsequently, small light spots merge, forming a single light spot, which blinks periodically from 0.56 min. At 1.12 min, an interference pattern emerges containing parallel lines in a circular area. To summarize, up to 1.12 min, we observe three events repeatedly: birefringence, sudden flashing of light for 0.01min, and finally, interference. Prior to the appearance of the first optical vortex in the projection camera, these three key observations suggest that three major events are occurring in the reaction vessel even before the

first nanowires (shown in the SEM image below) are formed. Since helical nanowires generate birefringence, the observation of birefringence can be associated with the initial formation of a helical structure (Figure S1). As noted above, the flash of light suggests the bonding of two large structures. Finally, the observation of an interference pattern signifies that the nucleation centers are around 600 nm in size, i.e. comparable to the wavelength of the incident light [20-21].

We match the reaction vessel camera visual with the projection camera output. The projection of the central beam reflected and refracted from the samples is captured by the projection camera on the wall. For the first time, we observe that the addition of the first angular momentum is at 1.12 min, and the ring remains stable until 1.20 min. This indicates that the helical nanowires observed in the first SEM images have already formed; otherwise, an optical vortex would not have been formed. Interference is caused by two entangled sources made by birefringence. Two events are observed before the first instance of helical nanowire formation. First, the flashing of light occurs at 0.22 min and 0.38 min. At 1.21 min, the refracted and the transmitted light that we monitor using the reaction vessel camera suddenly disappears as if there is no material in the reaction vessel. We call it a metastable state of the helical nanowire superstructure because, for 8-12 seconds, no diffraction e is visible in the reaction vessel camera.

We find a second phase transition in the reaction vessel video, 1.20 min to 2.57 min. The sizes of the particles are ~100 μm, which grows into a solid structure that refracts and transmits light in a nearly spherical shape at 2.57 min. The projection camera on the projection screen monitors reflected and transmitted lights. We find light rings with dark spots. Therefore, a photon with two angular momenta has been realized at 1.21 min.

At 3.07 min, the solid structure has been formed, and as we zoom out from the region, we find a large number of these structures start growing and colliding. Again, we refer to this as a metastable state.

At 3.19 min, we get a stable structure, the third and final condensate.

Visualization 4: Statistical database of repeated experiments. The video is a statistical database of independent syntheses of several optical condensate structures with three angular momenta under different mechanical perturbations. On the top part of the screen, two experiments are shown only to claim that the creation of a synthetic organic structure that leads to the formation of a stable optical structure is followed by massive turbulence in the solution (metastable state). At the lower part of the screen, the final optical vortex condensate has a designated number showing the code we have used for related data files; the code reflects a particular perturbation is applied to inhibit the formation of three condensates. It was presumed that if the reaction is perturbed, the nanowires will restructure, and the typical features of the optical superstructure would not be obtained. In other words, there is no optical sphere or any integrated photonic structure; the apparent optical sphere could be an illusion. What is observed as a 3D optical sphere is due to

interacting nanowires; if they are moved, we would never get the optical sphere. The relative positions of weakly bonded 3D nanowires are fixed. Multiple examples suggest that if perturbation remains within a critical limit, the final optical condensate structure or optical sphere remains intact.

Movie 4 summarizes various experiments, each with a code number using only one molecule (S)-Phenyl-hexadecanoylamino-acetic acid methyl ester. Here we have six columns. The first five columns have two videos in each column, and the sixth rightmost column has four videos in each column.

We carried out these 14 experiments of gel synthesis only to confirm whether the structural symmetry of one nanowire is intact under perturbation. We always obtain the optical sphere, irrespective of the degree and variety of perturbation applied to the solution. In the parenthesis below, we have noted the ultrasound signals pumped into the solution and changed chemical ratios between the precursor and the solvent so that the twisting parameters of the helical nanowire were changed. If the sphere is due to changes in the twisting parameters of the helical nanowires, then we should get similar kinds of optical vortices.

Here are the conditions in parenthesis with the video number.
The first column, video number 5592 (solution is perturbed with a stirrer as it cools and forms gel), 5603 (the solution is kept static in the beginning, after convergence, finally rotated to show that it is identical to 5592, which is an independent synthesis);
The second column, 5593 (solution is perturbed), 5593(static, after convergence, finally rotated to show that it is identical to 5593, which is an independent synthesis);
The third column, 5588 (ultrasound vibration 8MHz is injected into the solution), 5589(static, after convergence, initially rotated to show that it is identical to 5588, which is an independent synthesis, after rotation, the surface with no dark region is kept intact as a proof that such a stable surface cannot form by random structure);
The fourth column, 5590 (perturbed by hand using a stirrer), 5591(static, after convergence, finally rotated to show that it is identical to 5590, which is an independent synthesis);
Fifth column 2923(perturbed by shaking beaker using hand), 5604(static, after convergence, finally beaker is rotated to show that it is identical to 2923, which is an independent synthesis);
Sixth column, 5605 (static), 5601(static, after convergence, the beaker is finally rotated to show that it is identical to the other three independent syntheses), 5598(static, after convergence, finally beaker is rotated to show that it is identical to the other three independent syntheses), 5602(static, after convergence, finally beaker is rotated to show that it is identical to other three independent syntheses).

S5. References

1. Karnieli, A. & Arie, A. Fully controllable adiabatic geometric phase in nonlinear optics. *Opt. Express* **2018,** 26, 4920–4932.
2. Slussarenko, S. ; Alberucci, A.; Jisha, C.; et al. Guiding light via geometric phases. *Nature Photon* **2016**, 10, 571–575.
3. Kuznetsov, A.I.; Miroshnichenko, A.E.; Brongersma, M.L.; Kivshar, Y.S.; Luk'yanchuk, B. Optically resonant dielectric nanostructures. *Science* **2016**, 354(6314), 2472-1-7.
4. Wang, J. et al. Terabit free-space data transmission employing orbital angular momentum multiplexing. Nat. Photonics **2012**, 6, 488-496.
5. Bozinovic, N. et al. Terabit-Scale Orbital Angular Momentum Mode Division Multiplexing in Fibers. Science **2013**, 340, 1545–1548.
6. Maurer, C. ; Jesacher, A. ; Bernet, S. ; Ritsch-Marte, M. What spatial light modulators can do for optical microscopy. Laser Photonics Rev. **2011**, 5, 81–101.
7. Chakraborty, S.; Bhattacharya, K.; Sarkar, S. K. Quantitative birefringence microscopy with collinearly propagating orthogonally polarized beams. *Appl. Opt.* **2018**, 57, 1934–1939.
8. Mair, A.; Vaziri, A.; Weihs, G.; Zeilinger, A. Entanglement of the orbital angular momentum states of photons. *Nature* **2001**, **412**, 313–316.
9. Leach, J. et al. Quantum Correlations in Optical Angle-Orbital Angular Momentum Variables. Science **2010**, 329, 662–665.
10. Terech, P. ; Ostuni, E.; Weiss, R. G. Structural Study of Cholesteryl Anthraquinone-2-carboxylate (CAQ) Physical Organogels by Neutron and X-ray Small Angle Scattering. J. Phys. Chem. 1996, 100, 3759–3766.
11. Basak, S.; Nanda, J. ; Banerjee, A. A New Aromatic Amino Acid Based Organogel for Oil Spill Recovery. *J. Mater. Chem*. **2012**, 22, 11658–11664 .
12. Nagao, Y. ; Yagi, M. ; Ikede, T. ; Fujita, E. A New Chiral Recognition in Aminolysis of 3-Acyl-4(R)-methoxycarbonyl-1,3-thiazolidine-2-thione with Racemic Amines. *Tetrahedron Lett*. **1982**, 23, 201–204.
13. Ongaratto, R. ; et al. In Situ Formation of AuNPs using Fatty N-Acylamino Hydrazide Organogelators as Templates. *New. J. Chem*. **2019**, 43, 295–303.
14. Pal, A.; Ghosh, Y. K.; Bhattacharya, S. Molecular Mechanism of Physical Gelation of Hydrocarbons by Fatty Acid Amides of Natural Amino Acids. *Tetrahedron* **2007**, 63, 7334–7348.
15. Thalhammer, A. ; Mecinović, J. ; Schofield, C. J. ; Triflic Anhydride-mediated Synthesis of Oxazoles. *Tetrahedron Lett*. **2009**, 50, 1045–1047.
16. Ordóñez, M.; et al. A Convenient Method for the Preparation of Chiral Phosphonoacetamides and their Horner-Wadsworth-Emmons Reaction. Tetrahedron: Asymmetry **2007**, **18**, 2427–2436.
17. Bender, M. The use of light scattering to determine particle size and molecular weight and shape. J. Chem. Educ. **1952**, 29, 15–23.
18. Ye, Y. ; Pui, D. Y. H. Detection of nanoparticles suspended in a light scattering medium. Sci. Rep. **2011**, 11, 20268.
19. Kumar, A. ; Taneja, A. ; Mohanty, T. ; Singh, R. P. Effect of laser beam propagation through the plasmonic nanoparticles suspension. *Results in Optics* **2021**, 3**,** 100081.

20. Yang, Z. Y. ; Zhao, M. ; Lu, P. X.; Lu, Y. F. Ultrabroadband optical circular polarizers consisting of double-helical nanowire structures. *Opt. Lett.* **2010**, 35, 2588-2590.
21. Esposito, M. ; et al. Nanoscale 3D chiral plasmonic helices with circular dichroism at visible frequencies. *Acs Photonics* **2015**, 2 (1), 105-114.